

# Spontaneous symmetry breaking of dual-layer solitons in spin-orbit-coupled Bose-Einstein condensates

Zhaopin Chen<sup>1,\*</sup>, Yongyao Li<sup>2</sup>, Yan Liu<sup>3</sup>, and Boris A. Malomed<sup>4,5</sup>

<sup>1</sup>*Physics Department and Solid State Institute, Technion, Haifa 32000, Israel*

<sup>2</sup>*School of Physics and Optoelectronic Engineering, Foshan University, Foshan 52800, China*

<sup>3</sup>*Department of Applied Physics, South China Agricultural University, Guangzhou 510642, China*

<sup>4</sup>*Department of Physical Electronics, School of Electrical Engineering, Faculty of Engineering, Tel Aviv University, Tel Aviv 69978, Israel*

<sup>5</sup>*Instituto de Alta Investigación, Universidad de Tarapacá, Casilla 7D, Arica, Chile*

It is known that stable 2D solitons of the semi-vortex (SV) and mixed-mode (MM) types are maintained by the interplay of the cubic attractive nonlinearity and spin-orbit coupling (SOC) in binary Bose-Einstein condensates. We introduce a double-layer system, in which two binary condensates, stabilized by the SOC, are linearly coupled by tunneling. By means of the numerical methods, it is found that symmetric two-layer solitons undergo the spontaneous-symmetry-breaking (SSB) bifurcation of the *subcritical* type. The bifurcation produces families of asymmetric 2D solitons, which exist up to the value of the total norm equal to the norm of the Townes solitons, above which the collapse occurs. This situation terminates at a critical value of the inter-layer coupling, beyond which the SSB bifurcation is absent, as the collapse sets in earlier. Symmetric 2D solitons that are destabilized by the SSB demonstrate dynamical symmetry breaking, in combination with intrinsic oscillations of the solitons, or transition to the collapse, if the soliton's norm is sufficiently large. Asymmetric MMs produced by the SSB instability start spontaneous drift, in addition to the intrinsic vibrations. Consideration of moving 2D solitons is a nontrivial problem because SOC breaks the Galilean invariance. It is found that the system supports moving MMs up to a critical value of the velocity, beyond which they undergo delocalization.

## I. INTRODUCTION

Among many possibilities to realize new physics in Bose-Einstein condensates (BECs) created in ultracold atomic gases, well-known options are to use them as testbeds for emulation of various effects in condensed matter physics, which seem very complex in their original form [1]. In this context, great interest has been drawn to the experimentally demonstrated emulation of spin-orbit coupling (SOC) in the binary BEC. In its original form, SOC originates in physics of semiconductors, as the weakly relativistic interaction between the electron's magnetic moment and its motion through the electrostatic field of the ionic lattice [2, 3]. Mapping the electron's spinor wave function into the pseudo-spinor bosonic wave function of the binary condensate under the action of appropriate laser illumination, SOC is reproduced as the linear interaction between the pseudospin and momentum of bosonic atoms [4–8]. While a majority of experimental works on the SOC dealt with effectively one-dimensional (1D) SOC settings, the realization of the SOC in the two-dimensional (2D) BEC was reported too [9], which makes it relevant to consider 2D and, eventually, 3D SOC states.

The interplay of the linear SOC and usual intrinsic BEC nonlinearity with the repulsive sign was predicted to produce many nontrivial dynamical states: vortices [10–12], monopoles [13], skyrmions [14, 15], etc. Further, the similarity between the Gross-Pitaevskii equations (GPEs) for the spin-orbit-coupled binary condensate [16] and the model of the copropagation of orthogonal polarizations of light in twisted nonlinear optical fibers [17] helps to identify links between the nonlinear phenomenology in BEC and optics. In addition to that, the strong linear coupling of pseudospin 1/2 to the atomic momentum connects the physics of the spinor BEC to graphene physics and its emulation in photonic crystals [18].

It is natural to expect that solitons in binary condensates with the attractive sign of the intrinsic nonlinearity may be essentially affected by SOC. In the general case, a well-known problem is that, in the case of the cubic self-attraction, 2D fundamental (zero-vorticity,  $m = 0$ ) solitons are unstable in the free space, due to the occurrence of the critical collapse in this case [19–22], while solitons carrying integer vorticity  $m$  are subject to a still stronger splitting instability [23]. In particular, in the 2D case, the GPE with the cubic self-attraction term gives rise to degenerate families of fundamental Townes solitons (TSs) [24] and their vortical counterparts with  $m \geq 1$  [25–27].

---

\*Electronic address: zhaopin.chen@campus.technion.ac.il

The degeneracy means that the entire soliton family with given  $m$  shares a single value of the norm, which separates collapsing and decaying solutions. Therefore, the TSSs, that play the role of separatrices between these two types of the dynamical behavior, are completely unstable states. In turn, the degeneracy is a consequence of the specific scale invariance of the cubic GPE in two dimensions. Peculiarities of the onset of the critical collapse in the 2D SOC system were studied in Ref. [28].

A surprising result, which was first reported in Ref. [29], and further extended in works [30–32], is that two different families of solitons, namely *semi-vortices* (SVs, with topological charges  $m = 0$  and  $\pm 1$  separately carried by the two components) and *mixed modes* [MMs, which combine terms with  $m = (0, -1)$  and  $m = (0, +1)$  in the components] become *stable* in the 2D binary system with the self-attraction and linear SOC of the *Rashba type* [3, 33]. The SV (MM) solitons realize the ground state of the 2D system when the self-attraction in two components of the spinor wave function is stronger (weaker) than the cross-attraction between them. In the special case of the *Manakov's nonlinearity*, with equal strengths of the self- and cross-attraction [34], the SOC in the 2D system gives rise to a family of *composite solitons* (CSs), which continuously connects the SV and MM states with equal values of the norm and chemical potential, while the ratio of the norms of the two components, and their angular momenta, vary within the CS family [29, 30, 35]. The family is dynamically stable against small perturbations, but is subject to structural instability, as it is destroyed by any deviation from the Manakov's case.

The explanation of the stabilizing effect of the SOC for the 2D solitons in free space is provided by the fact that SOC sets up its length scale, which is inversely proportional to the SOC strength. This fixed length breaks the above-mentioned scale invariance, thus lifting the norm degeneracy of the solitons and pushing the norm *below* the threshold necessary for the onset of the critical collapse. Thus, being protected against the collapse, the solitons become stable modes that play the role of the system's ground state, which is missing in the scale-invariant 2D systems with the cubic self-attraction [29] (formally speaking, the collapsing mode is the ground state in the latter case).

Another topic of general interest in studies of nonlinear-wave systems is spontaneous symmetry breaking (SSB) between two waveguides (*cores*) with intrinsic nonlinearity (most frequently, it is cubic self-attraction), coupled by linear terms, which account for tunneling of photons or atoms in the optical or BEC realization of the system, respectively. For the first time, the onset of the SSB of 1D solitons in linearly coupled optical waveguides was predicted in Ref. [36], as the instability of symmetric solitons (ones with equal components in the coupled cores). The instability appears at a critical value of the nonlinearity strength, which is determined by the total norm of the soliton, see below. The analysis of solutions for the asymmetric 1D solitons, produced by the SSB beyond the critical point (and, actually, at values of the norm slightly smaller than the critical one, as the corresponding SSB bifurcation is of the *subcritical* type [37]) was developed in detail by means of numerical simulations and the variational approximation [38–41]. Experimental observation of the SSB of solitons in dual-core nonlinear optical fibers was reported only recently [42].

Similar predictions of the SSB phenomenology were developed for 1D matter-wave solitons in the double-layer BEC [43, 44]. Such a setting may be implemented in a deep symmetric double-well potential, each well trapping its layer of the self-attractive condensate; the layers are coupled by tunneling of atoms across a barrier separating the wells. This configuration was previously used in theoretical [45, 46] and experimental [47] studies of a related effect, *viz.*, spontaneous breaking of the *antisymmetry* of spatially odd continuous-wave states in the *self-repulsive* condensate.

In the case of the 2D double-layer self-attractive BEC, the first problem is the stabilization of each layer against the above-mentioned critical collapse. This may be provided by a spatially periodic lattice potential acting in the layers [43], or by the quadratic (harmonic-oscillator) trapping potential which is applied in each layer [48]. Then, the SSB gives rise to fundamental and vortical solitons (localized modes), with an asymmetric distribution of the atomic density between the coupler layers.

As mentioned above, the SOC readily stabilizes 2D solitons of the SV and MM types in the free space, without the use of any external potential. This property of the spin-orbit-coupled BEC suggests a possibility to predict the SSB between two components of the 2D solitons in the double-layer setting, which is the subject of the present work. We find that, similar to the above-mentioned situation, the solitons of the SV and MM types demonstrate subcritical bifurcations. However, the existence interval of asymmetric solitons in terms of the total norm,  $N$ , above the SSB critical value,  $N_{\text{cr}}$ , is small (somewhat similar to the situation in Ref. [48]) because the collapse threshold for strongly asymmetric 2D solitons is close to the TS norm,  $N_{\text{TS}}$ , while for symmetric solitons it is  $2N_{\text{TS}}$ .

The subsequent presentation is structured as follows. The double-layer SOC system is introduced in Section II, where we also represent its linear spectrum. This is followed in Section III by a detailed analysis of families of symmetric and asymmetric 2D solitons in the double-layer system. Stationary solutions of SV, MM, and composite types are constructed by means of the accelerated imaginary-time evolution method (AITEM) [49] with mesh number  $N_x = N_y = 256$ . Stability of the solutions is identified by means of systematic simulations of their perturbed evolution, with a total evolution time  $t = 400$ . The results are reported in a systematic form for two-layer solitons of the SV and MM types, and briefly for CSs in the special case of the Manakov's nonlinearity. Section IV addresses moving 2D solitons. This is a nontrivial problem, as SOC destroys the system's Galilean invariance, making it impossible to construct moving modes as boosted copies of quiescent ones.

## II. THE DOUBLE-LAYER SOC MODEL

We consider the system modeled by two pairs of spin-orbit-coupled 2D GPEs, with spatial coordinates  $(x, y)$ , for two parallel layers of the two-component BEC:

$$\begin{aligned}
i\frac{\partial\phi_+}{\partial t} &= -\frac{1}{2}\nabla^2\phi_+ - (|\phi_+|^2 + \gamma|\phi_-|^2)\phi_+ + \lambda\left(\frac{\partial\phi_-}{\partial x} - i\frac{\partial\phi_-}{\partial y}\right) - \kappa\psi_+, \\
i\frac{\partial\phi_-}{\partial t} &= -\frac{1}{2}\nabla^2\phi_- - (|\phi_-|^2 + \gamma|\phi_+|^2)\phi_- - \lambda\left(\frac{\partial\phi_+}{\partial x} + i\frac{\partial\phi_+}{\partial y}\right) - \kappa\psi_-, \\
i\frac{\partial\psi_+}{\partial t} &= -\frac{1}{2}\nabla^2\psi_+ - (|\psi_+|^2 + \gamma|\psi_-|^2)\psi_+ + \lambda\left(\frac{\partial\psi_-}{\partial x} - i\frac{\partial\psi_-}{\partial y}\right) - \kappa\phi_+, \\
i\frac{\partial\psi_-}{\partial t} &= -\frac{1}{2}\nabla^2\psi_- - (|\psi_-|^2 + \gamma|\psi_+|^2)\psi_- - \lambda\left(\frac{\partial\psi_+}{\partial x} + i\frac{\partial\psi_+}{\partial y}\right) - \kappa\phi_-,
\end{aligned} \tag{1}$$

where  $\phi_{\pm}$  and  $\psi_{\pm}$  are components of the mean-field wave functions in the two layers,  $\kappa > 0$  is the coefficient of the tunnel coupling between them, and  $\gamma \geq 0$  is the relative strength of the attractive interaction between the components in each layer, while the self-attraction coefficient is scaled to be 1. Following Ref. [29], SVs and MMs are considered, respectively, for  $\gamma = 0$  and  $\gamma = 2$ . Real coefficient  $\lambda$  is the strength of the SOC of the Rashba type in each layer. The remaining scaling invariance of the system makes it possible to set  $\lambda = 1$  (keeping  $\kappa$  as a control parameter), therefore numerical results are presented below for this value.

The total energy of the system includes terms accounting for the kinetic energy, nonlinearity, SOC, and inter-layer coupling:

$$E = E_{\text{kin}} + E_{\text{int}} + E_{\text{soc}} + E_{\text{coupl}}, \tag{2}$$

where

$$E_{\text{kin}} = \frac{1}{2} \iint \sum_{+,-} (|\nabla\phi_{\pm}|^2 + |\nabla\psi_{\pm}|^2) dx dy, \tag{3}$$

$$E_{\text{int}} = -\frac{1}{2} \iint \left[ \sum_{+,-} (|\phi_{\pm}|^4 + |\psi_{\pm}|^4) + 2\gamma (|\phi_+|^2|\phi_-|^2 + |\psi_+|^2|\psi_-|^2) \right] dx dy, \tag{4}$$

$$E_{\text{soc}} = \lambda \iint \left[ \phi_+^* \left( (\phi_-)_x - i(\phi_-)_y \right) + \psi_+^* \left( (\psi_-)_x - i(\psi_-)_y \right) \right] dx dy + \text{c.c.}, \tag{5}$$

$$E_{\text{coupl}} = -\kappa \sum_{+,-} \iint \phi_{\pm}^* \psi_{\pm} dx dy + \text{c.c.}, \tag{6}$$

with c.c. standing for the complex-conjugate expression.

Looking for a solution to the linearized form of Eq. (1) in the form of

$$\phi_{\pm}, \psi_{\pm} \sim \exp(-i\mu t + p_x x + p_y y) \tag{7}$$

leads to the set of four branches of the relation between chemical potential  $\mu$  and wavenumbers  $p_{x,y}$  defined in Eq. (7):

$$\mu = \frac{1}{2}p^2 \pm \lambda p - \kappa, \mu = \frac{1}{2}p^2 \pm \lambda p + \kappa, \tag{8}$$

where  $p = \sqrt{p_x^2 + p_y^2}$ . This result determines the *semi-infinite gap*, in terms of  $\mu$ , which is not covered by Eq. (8), hence it may be populated by solitons:

$$\mu < \mu_{\text{min}} \equiv -\frac{1}{2}\lambda^2 - \kappa, \tag{9}$$

where the minimum value of  $\mu(p)$  is attained at  $p = \lambda$ .

Stationary states with chemical potential  $\mu$  are looked for as solutions to Eq. (1) in the form of

$$\phi_{\pm}(x, y, t) = \Phi_{\pm}(x, y)e^{-i\mu t}, \psi_{\pm}(x, y, t) = \Psi_{\pm}(x, y)e^{-i\mu t}, \quad (10)$$

where stationary wave functions satisfy equations

$$\begin{aligned} \mu\Phi_+ &= -\frac{1}{2}\nabla^2\Phi_+ - (|\Phi_+|^2 + \gamma|\Phi_-|^2)\Phi_+ + \lambda\left(\frac{\partial\Phi_-}{\partial x} - i\frac{\partial\Phi_-}{\partial y}\right) - \kappa\Psi_+, \\ \mu\Phi_- &= -\frac{1}{2}\nabla^2\Phi_- - (|\Phi_-|^2 + \gamma|\Phi_+|^2)\Phi_- - \lambda\left(\frac{\partial\Phi_+}{\partial x} + i\frac{\partial\Phi_+}{\partial y}\right) - \kappa\Psi_-, \\ \mu\Psi_+ &= -\frac{1}{2}\nabla^2\Psi_+ - (|\Psi_+|^2 + \gamma|\Psi_-|^2)\Psi_+ + \lambda\left(\frac{\partial\Psi_-}{\partial x} - i\frac{\partial\Psi_-}{\partial y}\right) - \kappa\Phi_+, \\ \mu\Psi_- &= -\frac{1}{2}\nabla^2\Psi_- - (|\Psi_-|^2 + \gamma|\Psi_+|^2)\Psi_- - \lambda\left(\frac{\partial\Psi_+}{\partial x} + i\frac{\partial\Psi_+}{\partial y}\right) - \kappa\Phi_-, \end{aligned} \quad (11)$$

The stationary states are characterized by the total norm,

$$N = N_{\phi} + N_{\psi} \equiv N_{\phi_+} + N_{\phi_-} + N_{\psi_+} + N_{\psi_-} = \iint (|\Phi_+|^2 + |\Phi_-|^2 + |\Psi_+|^2 + |\Psi_-|^2) dx dy. \quad (12)$$

The SSB in the present system is quantified by means of the norm difference between the layers,

$$\theta = \frac{|N_{\phi} - N_{\psi}|}{N_{\phi} + N_{\psi}}. \quad (13)$$

In the single-layer system ( $\kappa = 0$ ,  $\psi_{\pm} = 0$ ), the family of SV solitons with  $\gamma < 1$  is completely stable. It exists in the interval of

$$0 < N < N_{\text{TS}} \approx 5.85, \quad (14)$$

which corresponds to  $\mu < -\lambda^2/2$  [see Eq. (9)], where  $N_{\text{TS}}$  is the norm of the single-component TS. In the limit of  $\mu \rightarrow -\infty$ , the two-component SV degenerates into a single-component TS [29, 32]. The MM solitons are unstable at  $\gamma < 1$ .

In the case of  $\gamma > 1$ , the SVs are unstable, while the MM family is completely stable in the single layer. This family exists in the interval of norms

$$0 < N < 2N_{\text{TS}}/(\gamma + 1). \quad (15)$$

In the limit of  $\mu \rightarrow -\infty$ , the MM state turns into a symmetric two-component TS, which corresponds to the largest norm in Eq. (15).

There exist two isomers of the SV-type solitons, with right- and left-handed chiralities, which are defined, respectively, by vorticity sets  $(S_+, S_-) = (0, +1)$  and  $(\bar{S}_+, \bar{S}_-) = (-1, 0)$  in the two components [35]. Numerical solutions for them are produced, severally, by the following inputs:

$$\phi_+^{(0)} = A_1 \exp(-\alpha_1 r^2), \phi_-^{(0)} = A_2 r \exp(i\theta - \alpha_2 r^2), \quad (16)$$

$$\overline{\phi_+^{(0)}} = -A_2 r \exp(-i\theta - \alpha_2 r^2), \overline{\phi_-^{(0)}} = A_1 \exp(-\alpha_1 r^2), \quad (17)$$

which are written in polar coordinates  $(r, \theta)$ , with real  $A_{1,2}$  and  $\alpha_{1,2} > 0$ . The creation of MMs and CSs is initiated by a combination of inputs (16) and (17) with the opposite chiralities,

$$\phi_{\pm} = M\phi_{\pm}^{(0)} + \sqrt{1 - M^2} \cdot \overline{\phi_{\pm}^{(0)}}, \quad (18)$$

where the weight factor takes values  $-1 \leq M \leq 1$ . The choice of  $|M| = 1/\sqrt{2}$  in Eq. (18) corresponds to MMs, while  $|M| \neq 0, 1/\sqrt{2}$  corresponds to CSs (in the case of  $\gamma = 1$ ). In our double-layer system, the symmetric and asymmetric solutions can be generated by setting the initial norms in the layers as  $N_{\phi} = N_{\psi}$  and  $N_{\phi} \neq N_{\psi}$ , respectively.

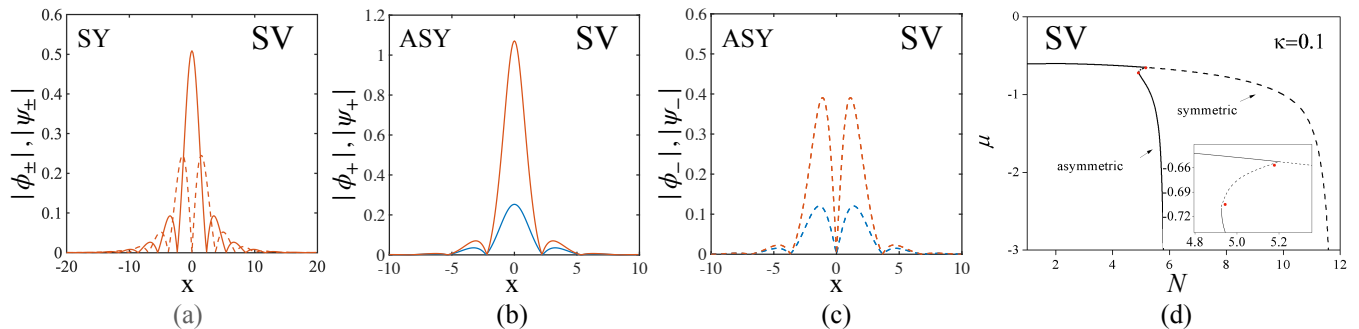


FIG. 1: (Color online) (a) Cross-section profiles, drawn along  $y = 0$ , of a stable symmetric semi-vortex (SV) with  $\gamma = 0$  in Eqs. (1), total norm  $N = 5$ , and inter-layer coupling constant  $\kappa = 0.1$ . The solid and dashed lines represent, respectively,  $|\phi_+| = |\psi_+|$  and  $|\phi_-| = |\psi_-|$ . Here and in other figures, labels SY and ASY pertain, respectively, to symmetric and asymmetric solitons in the double-layer system. Panels (b) and (c) separately display the profiles (solid and dashed, for  $\phi_+, \psi_+$  and  $\phi_-, \psi_-$ , respectively) for a stable asymmetric SV, with the same values of  $N$  and  $\kappa$ . In panels (b) and (c), blue and orange curves represent, respectively,  $|\phi_{\pm}|$  and  $|\psi_{\pm}|$  components, with the broken symmetry between the coupled layers ( $|\phi_{\pm}| \neq |\psi_{\pm}|$ ). These symmetric and asymmetric SVs belong to the bistability region, see Eq. (19). (d) The chemical potential,  $\mu$ , vs. the total norm,  $N$ , for the families of the symmetric and asymmetric SV solitons. Here, the solid and dashed curves designate stable and unstable solutions, respectively. Red dots denote the symmetry-breaking bifurcation point, at  $N = N_{\text{cr}}$ , and the turning point, at  $N = N_{\text{turn}}$ , of the  $\mu(N)$  curve for the asymmetric family, see Eq. (19). The inset provides a zoom of the area around the symmetry-breaking bifurcation.

### III. SYMMETRIC AND ASYMMETRIC SOLITONS IN THE DOUBLE-LAYER SYSTEM

#### A. Semi-vortices

Basic numerical findings for SV solitons are displayed in Figs. 1 and 3 [recall the numerical results are produced setting  $\lambda = 1$  in Eqs. (1)]. First, typical shapes of stable SVs, which are symmetric and asymmetric with respect to the two layers, are displayed, by means of their 1D cross sections, in Figs. 1(a) and (b,c), respectively. 2D profiles of the same asymmetric SV which is presented in Figs. 1(b,c) are displayed in Fig. 2. They feature a maximum at the center ( $x = y = 0$ ) in the  $(\phi_+, \psi_+)$  components, and zero at the same point in the  $(\phi_-, \psi_-)$  ones, in accordance with the basic structure of the SV: it contains a zero-vorticity mode in  $(\phi_+, \psi_+)$ , and a vortical one in  $(\phi_-, \psi_-)$ .

Families of stable and unstable symmetric and asymmetric SV modes are represented by curves showing the modes' chemical potential,  $\mu$ , vs. their total norm (12) in Fig. 1(d). Note that the short segment of the asymmetric family, between the SSB point and the turning one, features  $d\mu/dN > 0$ , while its extension, in the form of the long segment below the turning point, has  $d\mu/dN < 0$ . In agreement with the Vakhitov-Kolokolov (VK) criterion, which is a well-known necessary stability condition [20–22, 50], these segments represent, respectively, unstable and stable states. The entire branch of the symmetric SV solitons satisfies the VK criterion, but it is unstable against SSB above the critical point (the latter instability cannot be captured by the VK criterion). As is typical for subcritical bifurcations [37], the interval of values of the norm,

$$N_{\text{turn}} < N < N_{\text{cr}}, \quad (19)$$

between the turning and critical (bifurcation) points maintains bistability, as both the symmetric and asymmetric states are stable in it.

The branch of the symmetric solitons naturally terminates at the point of

$$N = 2N_{\text{TS}}, \quad (20)$$

with norm  $N_{\text{TS}}$  in each layer. On the other hand, the branch representing the asymmetric solitons terminates when the asymmetry parameter (13) attains the limit,  $\theta = 1$ , i.e., one layer becomes empty and, accordingly, the respective total norm is  $N = N_{\text{TS}}$ . Comparison of Fig. 1(d) with the known value  $N_{\text{TS}} \approx 5.85$  [see Eq. (14)] corroborates these expectations.

The SSB bifurcation in the double-layer systems is characterized by the dependence of the asymmetry parameter (13) on the full norm (12) [38]–[44]. It is displayed in Fig. 3 for the two-layer solitons of the SV type with two different values of the inter-layer coupling constant, *viz.*,  $\kappa = 0.05$  (a) and  $\kappa = 0.1$  (b). It is obvious that the bifurcation is of the subcritical type, featuring the turning point on the  $\theta(N)$  curves, and narrow bistability regions identified as per

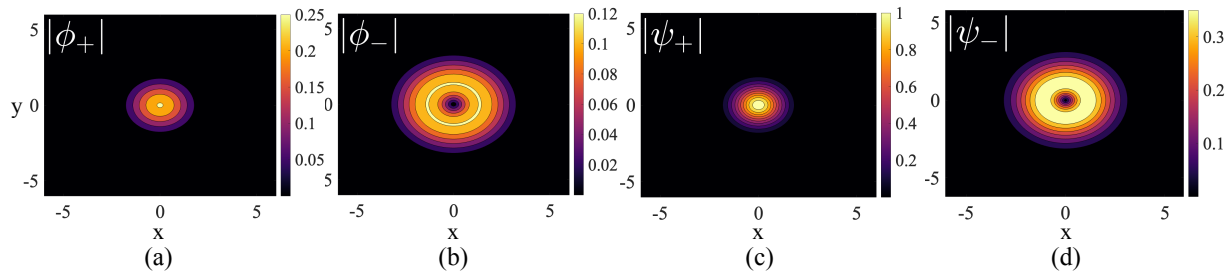


FIG. 2: (Color online) (a) Top-view profiles of the absolute value of the zero-vorticity (a,c) and vortical (b,d) components of the same stable asymmetric SV which is represented by its cross-section profiles in Figs. 1(b,c).

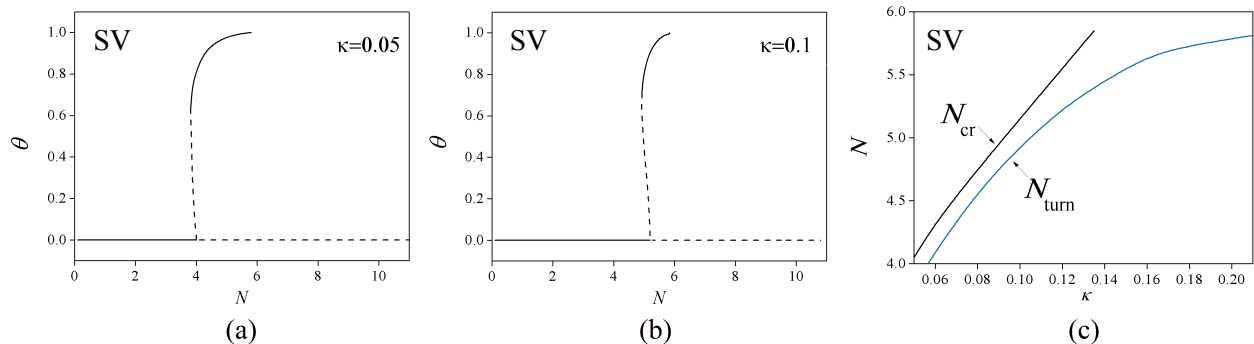


FIG. 3: (Color online) (a,b) The dependence of the asymmetry parameter (13) on the total norm (12) for the two-layer 2D solitons of the SV type, with  $\gamma = 0$  in Eqs. (1) and values of the inter-layer coupling  $\kappa = 0.05$  (a) or  $\kappa = 0.1$  (b). Solid and dashed curves designate stable and unstable families of the solutions, respectively. (c) The value of the norm at the turning point,  $N_{\text{turn}}$ , at which the asymmetric SV states are created by the subcritical bifurcation, and the critical norm,  $N_{\text{cr}}$ , at which the symmetric SV solution becomes unstable, vs.  $\kappa$ . The system is bistable, featuring the coexistence of stable symmetric and asymmetric states, in the region of  $N_{\text{turn}} < N < N_{\text{cr}}$ , see Eq. (19).

Eq. (19). The numerical results produce similar  $\theta(N)$  curves at other values of  $\kappa$  – in particular, the bifurcation never becomes supercritical, in which the curve would not go backward, and no bistability would be observed. Overall, the subcritical SSB bifurcation is described by dependences  $N_{\text{turn}}(\kappa)$  and  $N_{\text{cr}}(\kappa)$ , which are displayed in Fig. 3(c). The entire bistability region is located between these two curves. All the curves shown in Fig. 3 for the asymmetric families terminate at the above-mentioned point,  $N = N_{\text{TS}} \approx 5.85$ , at which the critical collapse sets in. The collapse does not admit the existence of stationary solitons at  $N > N_{\text{TS}}$ .

In direct simulations, unstable symmetric solitons of the SV type with the total norm falling in interval

$$N_{\text{cr}} < N < N_{\text{TS}} \quad (21)$$

(hence the collapse cannot commence in the system) demonstrate dynamical symmetry breaking, spontaneously transforming into oscillatory states (breathers) which keep the original structure of the SV soliton, i.e., the zero-vorticity and vorticity-1 shapes of their larger and smaller components, while the overall amplitude of the SV mode spontaneously becomes higher in one layer than in the other. A typical example of such a breather with the spontaneously broken inter-layer symmetry is displayed in Fig. 4. This dynamical regime may be considered as Josephson oscillations in the bosonic junction, cf. Refs. [45–47]. The oscillations proceed out-of-phase in the tunnel-coupled layers, i.e., a maximum amplitude in one layer coincides, in time, with a minimum in the other one. Naturally, the oscillation frequencies grow with the increase of the solitons’ norm. Detailed results of the simulations demonstrate that the spontaneously established oscillations are accompanied by generation of dispersive waves (“radiation”) with very small amplitudes. The radiation is virtually invisible in Fig. 4, and remained invisible as long as the simulations were running.

The outcome of the development of the spontaneously initiated dynamical symmetry breaking is different in the interval of

$$N_{\text{TS}} < N < 2N_{\text{TS}}. \quad (22)$$

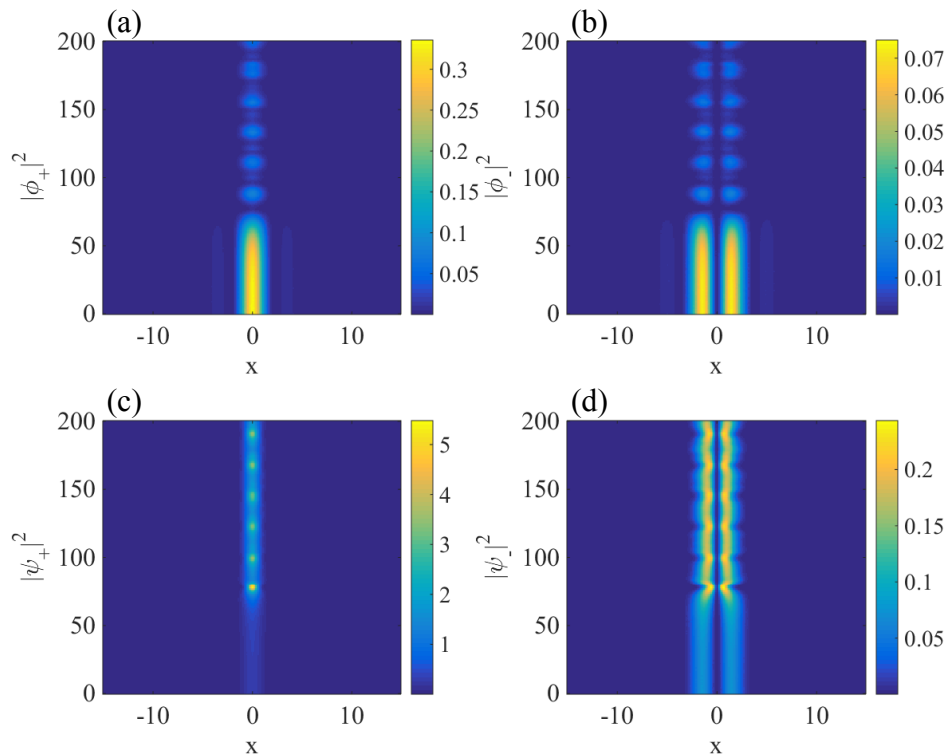


FIG. 4: (Color online) The numerically simulated evolution of an unstable symmetric SV (shown by density cross-sections of its components along  $y = 0$ ) with  $\kappa = 0.1$  and  $N = 5.6$ . The evolution exhibits the onset of the SSB (spontaneous symmetry breaking) with concomitant Josephson oscillations. Note that these values of the parameters belong to interval (21). Note also that widely different scales are used for plotting the component densities in the two layers,  $|\phi_{\pm}|^2$  and  $|\psi_{\pm}|^2$ , because the SSB makes their amplitudes strongly different.

Instead of the oscillations, the growth of the norm in one layer allows it to reach the collapse threshold, which indeed leads to the blowup of the fields, see Fig. 5.

It is relevant to stress the SSB for SVs takes place in a finite interval of the values of the coupling constant,

$$0 < \kappa < \kappa_{\max}^{(\text{SV})} \approx 0.135, \quad (23)$$

with  $\kappa_{\max}^{(\text{SV})}$  determined by the condition that the SSB occurs at  $N = N_{\text{TS}}$ , i.e., by equation

$$N_{\text{cr}}(\kappa_{\max}^{(\text{SV})}) = N_{\text{TS}}, \quad (24)$$

see Fig. 3(c). At  $\kappa > \kappa_{\max}^{(\text{SV})}$ , the critical collapse occurs prior to the expected onset of the SSB.

As concerns unstable asymmetric states existing in interval (19), which are shown by dashed segments of the respective curves  $\mu(N)$  in Fig. 1(d) and  $\theta(N)$  in Figs. 3(a,b), direct simulations demonstrate that, depending on values of the parameters and small perturbations which initiate the growth of the instability, they evolve into breathers which oscillate around either the stable symmetric state or stable asymmetric one, coexisting with its symmetric counterpart in the bistability region (19). A typical example of the oscillation instability is shown in Fig. 6.

## B. Mixed modes

Typical examples of amplitude profiles in stable symmetric and asymmetric MMs are plotted, by means of the cross sections along  $y = 0$ , in Figs. 7(a) and (b,c), respectively. 2D profiles of the same asymmetric MM which is presented in Figs. 7(b,c) are displayed in Fig. 8. Note that, while the system spontaneously breaks the symmetry between the

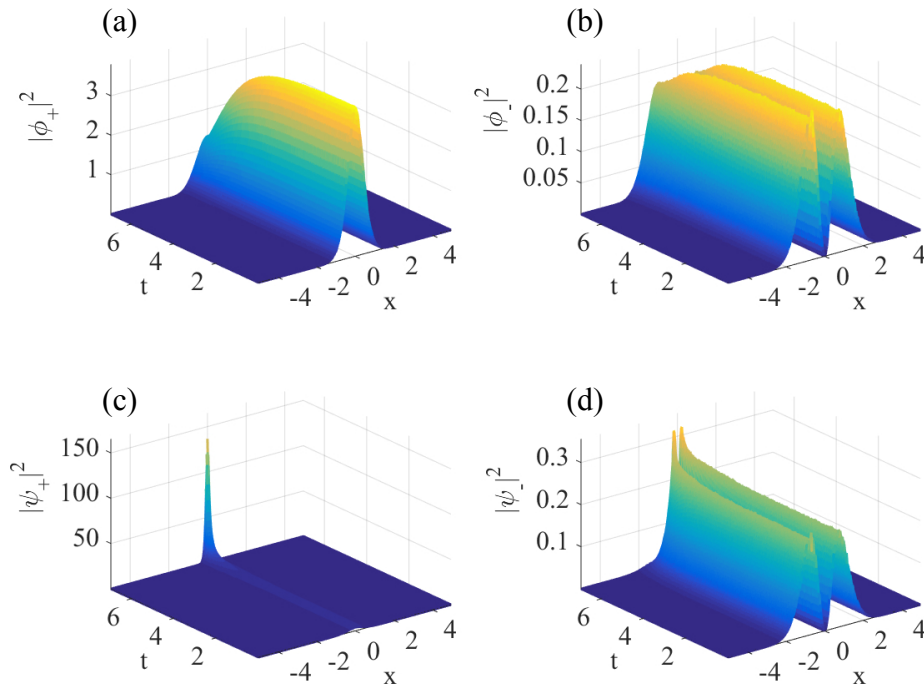


FIG. 5: (Color online) The evolution of an unstable symmetric SV (shown by means of the density cross-sections along  $y = 0$ ) with  $\kappa = 0.1$  and  $N = 11$ . The latter value falls in interval (22), where the collapse may take place in a single layer, which indeed happens here. To display the evolution of the intensities in the two layers, very different scales are used in the plots for  $|\phi_{\pm}|^2$  and  $|\psi_{\pm}|^2$ .

tunnel-coupled layers, the solutions keep the cross symmetries of Eqs. (11) with respect to the following substitution:  $\{\Phi, \Psi\}_+ \longleftrightarrow \{\Phi, \Psi\}_-, x \rightarrow -x$ , and  $\{\Phi, \Psi\}_+ \longleftrightarrow -\{\Phi, \Psi\}_-, y \rightarrow -y$ .

Dependences  $N(\mu)$  for the two-layer MM states are displayed in Fig. 7(d). Note that the VK criterion, if applied to these dependences, produces essentially the same conclusions as reported above for the SV families shown in Fig. 1. The straightforward consideration which is also similar to that presented above for the SVs demonstrates that the asymmetric MM states exist in the interval of values of the total norm given by Eq. (15), which is bounded by the onset of the collapse in the single layer, while the symmetric MM solitons exist in the interval which is twice as broad, *viz.*,  $0 < N < 4N_{\text{TS}}/(\gamma + 1)$ , cf. Eq. (20).

The SSB bifurcation for the MM states is also of the subcritical type, as shown in Figs. 9(a,b). Similar to the case of the SVs, the bifurcation for the MMs is characterized by dependences  $N_{\text{turn}}(\kappa)$  and  $N_{\text{cr}}(\kappa)$ , with the bistability region bounded by these curves, as shown in Fig. 9(c).

Figure 9(c) demonstrates that the SSB for MMs takes place in a finite interval of the values of the inter-layer coupling constant,

$$0 < \kappa < \kappa_{\text{max}}^{(\text{MM})} \approx 0.23 \quad (25)$$

[cf. Eq. (23) for the SV states], with  $\kappa_{\text{max}}^{(\text{MM})}$  determined by the condition

$$N_{\text{cr}}\left(\kappa_{\text{max}}^{(\text{MM})}\right) = 2N_{\text{TS}}/(1 + \gamma), \quad (26)$$

cf. Eq. (24). At  $\kappa > \kappa_{\text{max}}^{(\text{MM})}$ , the SSB does not take place, as the critical collapse occurs earlier. Accordingly, all curves for asymmetric MMs in Fig. 9 terminate at  $N = (2/3)N_{\text{TS}}$ , which corresponds to the value in Eq. (26) at  $\gamma = 2$ .

It is worthy to note that the existence region of the SSB for the MM solitons, as given by Eq. (25) is essentially broader than the similar region for the SV states, given by Eq. (23).



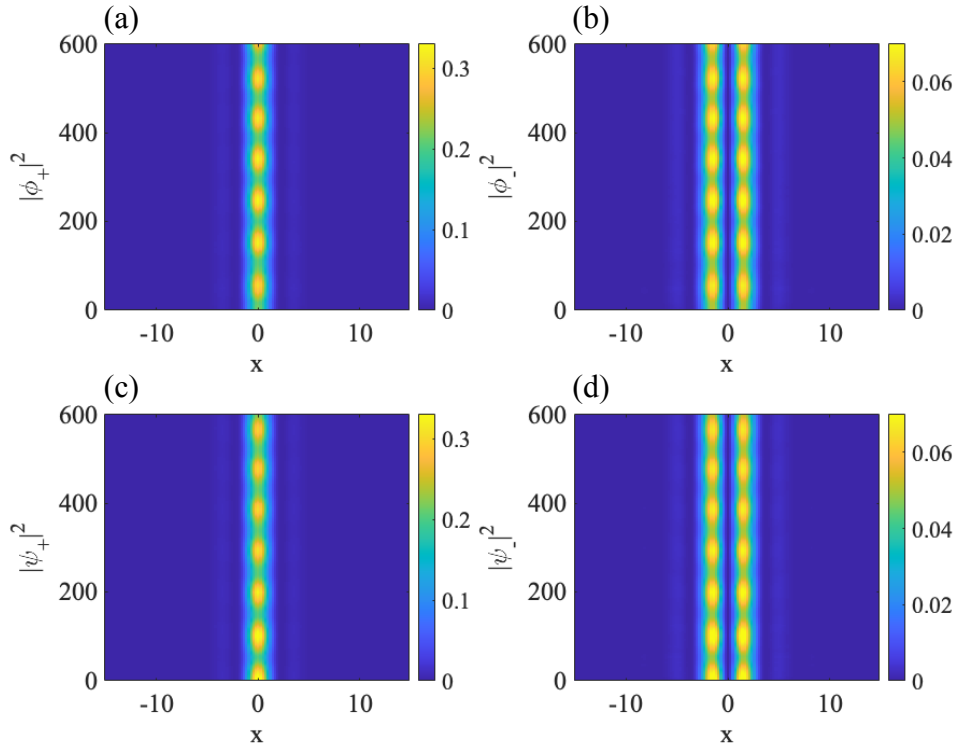


FIG. 6: (Color online) The numerically simulated evolution of an unstable asymmetric SV (shown by the density cross-section along  $y = 0$ ) with  $\kappa = 0.1$  and  $N = 5.12$ . Note that this value belongs to interval (21). The evolution exhibits the spontaneous transformation of the unstable SV into a breather oscillating around the stable symmetric SV.

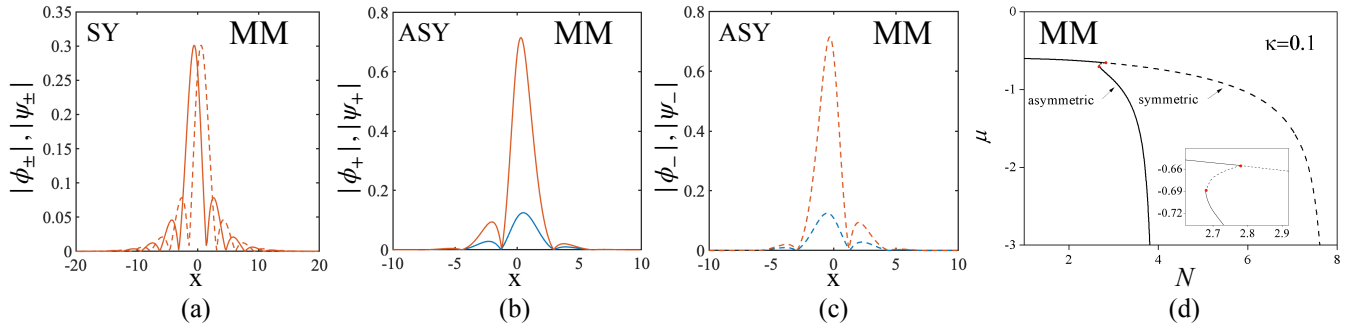


FIG. 7: (Color online) (a) Cross-section profiles, along axis  $y = 0$ , of a stable symmetric MM (mixed mode) with  $\gamma = 2$  in Eqs. (1), total norm  $N = 2.7$ , and the inter-layer coupling constant  $\kappa = 0.1$ . Solid and dashed lines designate, respectively,  $|\phi_+| = |\psi_+|$  and  $|\phi_-| = |\psi_-|$ . (b,c) The same profiles (solid and dashed for  $\phi_+, \psi_+$  and  $\phi_-, \psi_-$ , respectively) for a stable asymmetric MM with  $N = 3$  and  $\kappa = 0.1$ . Here blue and orange curves represent, respectively, the  $\phi_{\pm}$  and  $\psi_{\pm}$  components. (d)  $N(\mu)$  dependences for the families of symmetric and asymmetric two-layer states of the MM type. In this panel, solid and dashed curves stand for stable and unstable solutions, respectively. Dots denote the symmetry-breaking bifurcation point, and the turning point of the  $\mu(N)$  curve for the asymmetric family. The inset provides a zoom of the area around the bifurcation, cf. Fig. 1 for the SV states.

Direct simulations, displayed in Fig. 10, demonstrates that the symmetry-breaking instability of symmetric MM solitons, which exist in the interval of

$$N_{cr} < N < 2N_{TS}/(1 + \gamma), \quad (27)$$

gives rise to breathers, accompanied by the emission of very weak dispersive waves (practically invisible in Fig. 10). Their behavior is very different from that of the breathers generated by the instability of the symmetric states of

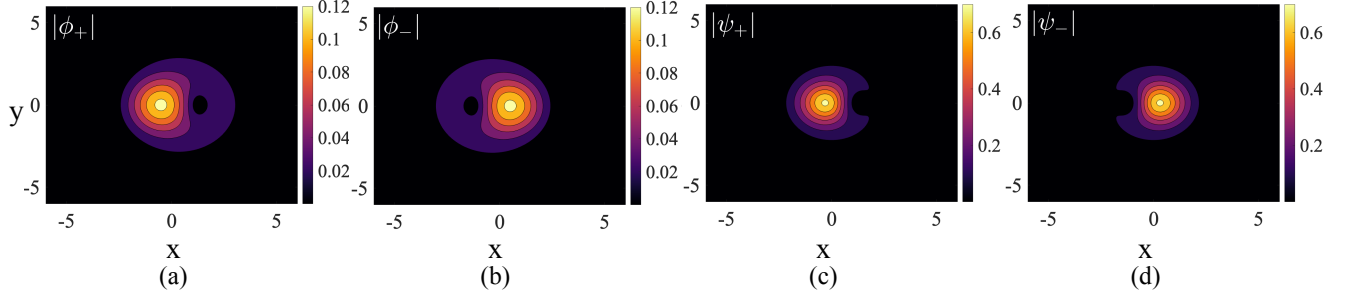


FIG. 8: (Color online) Top-view profiles of the components of the asymmetric MM which is presented by its cross-section profiles in Figs. 7 (b,c), cf. Fig. 2 for the asymmetric SV.

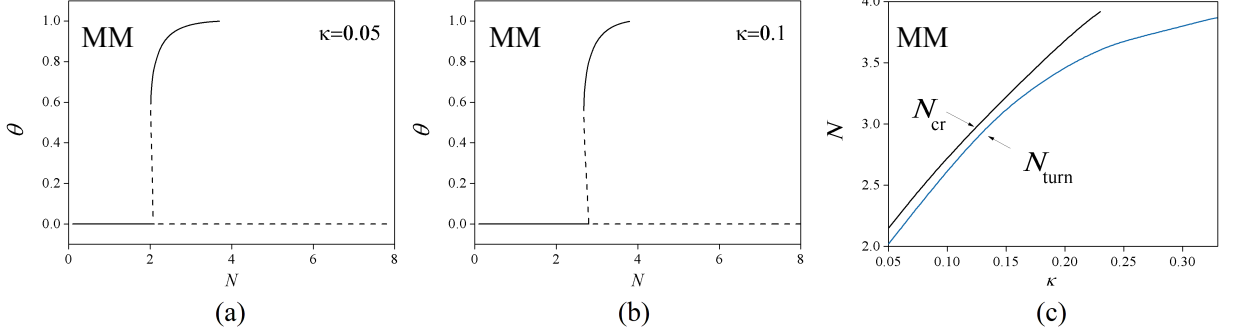


FIG. 9: (Color online) The subcritical SSB bifurcation of 2D two-layer MMs, for  $\gamma = 2$  in Eqs. (1) and  $\kappa = 0.05$  (a) or  $\kappa = 0.1$  (b), is illustrated by dependences of asymmetry (13) on the total norm (12), cf. Figs. 3(a,b). Solid and dashed curves designate stable and unstable solutions, respectively. (c) The value of the norm at the turning point,  $N_{\text{turn}}$ , at which the asymmetric MM states are created by the subcritical bifurcation, and the critical norm,  $N_{\text{cr}}$ , at which the symmetric MM solution becomes unstable, vs.  $\kappa$ . The system is bistable, featuring the coexistence of stable symmetric and asymmetric states, in the region of  $N_{\text{turn}} < N < N_{\text{cr}}$ , cf. Fig. 3(c) for the two-layer SV solitons.

the SV type, cf. Fig. 4. Indeed, along with the intrinsic oscillations, the breathers of the MM type feature slow *spontaneous drift*, which is clearly seen in Fig. 10. The trend of unstable MMs to develop spontaneous drift is also known in other cases [29].

In addition to interval (27), unstable symmetric MMs exist also in the range of

$$2N_{\text{TS}}/(1+\gamma) < N < 4N_{\text{TS}}/(1+\gamma), \quad (28)$$

where the collapse may commence in a single layer, cf. a similar interval (22) for the SV solitons. Accordingly, in this case the development of the SSB leads to the collapse, as shown in Fig. 11, similar to what happens with the unstable symmetric SV soliton in Fig. 5.

### C. Composite solitons

As well as its single-layer counterpart [29], the present system with  $\gamma = 1$  in Eqs. (1) supports a continuous family of CS states connecting the SV and MM solutions with equal values of  $N$  and  $\mu$ . Typical examples of stable symmetric and asymmetric CSs are displayed in Figs. 12(a) and (b,c), respectively, with the top views of the component distribution in the latter one plotted in Fig. 13.

As mentioned above, the CS family is a degenerate one, in the sense that all solutions belonging to it share a single value of the total norm, as well as a single value of the chemical potential. Within the family, the solutions differ by values of the angular momentum per particle in each component,

$$L_{(\phi,\psi)\pm} = N_{\pm}^{-1} \int \int (\phi, \psi)_{\pm}^* \hat{\mathcal{L}}_z (\phi, \psi)_{\pm} dx dy, \quad (29)$$

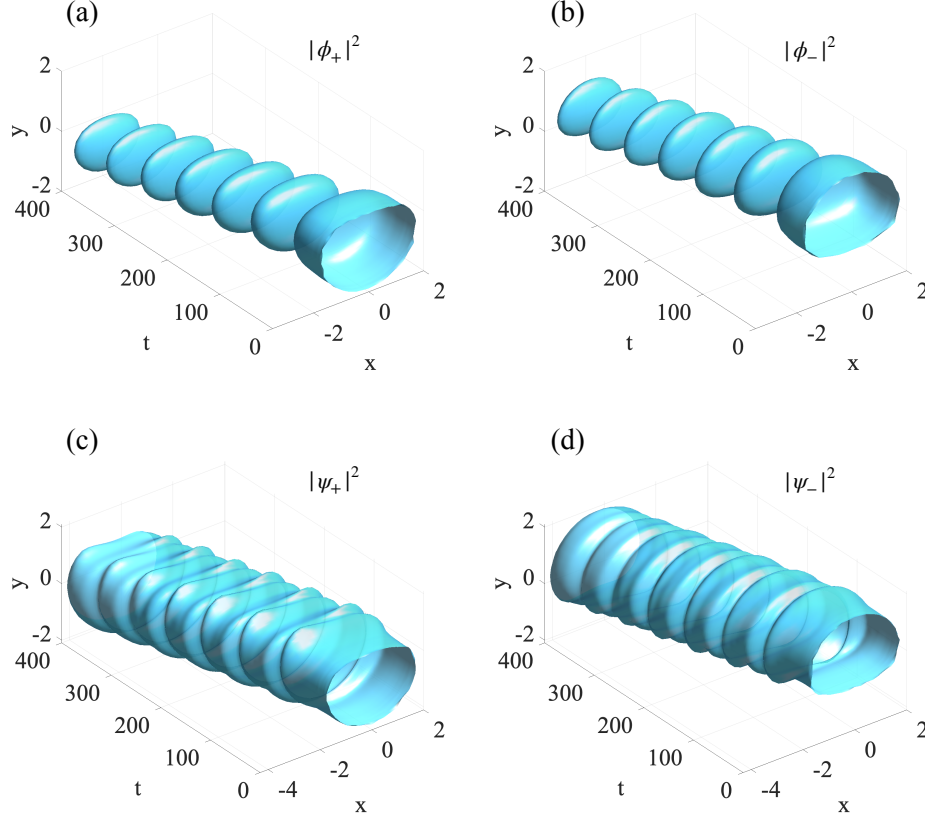


FIG. 10: (Color online) The evolution of an unstable symmetric MM, with  $\gamma = 2$ ,  $\kappa = 0.1$ , and  $N = 3$ , which belongs to interval (27). The spontaneously established intrinsic oscillations and slow drift of the two-layer 2D soliton are displayed by means surface plots  $|\phi_{\pm}(x, y)|^2 = |\psi_{\pm}(x, y)|^2 = 0.03$ .

with  $\hat{\mathcal{L}}_z = -i(x\partial/\partial y - y\partial/\partial x) \equiv -i\partial/\partial\eta$ , where  $\eta$  is the angular coordinate in the  $(x, y)$  plane.

Taking into regard that  $2/(1 + \gamma) = 1$  for  $\gamma = 1$ , Eqs. (15) and (20) predict that the symmetric and asymmetric CS families exist in intervals  $0 < N < 2N_{\text{TS}}$  and  $N < N_{\text{TS}}$ , respectively. These predictions are corroborated by numerical simulations. The numerical results for symmetric and asymmetric CS modes, including the  $\mu(N)$  and  $\theta(N)$  dependences, and conclusions concerning the evolution of unstable states, are quite similar to those reported above for the SV and MM states in Figs. 1(d)-5 and (7(d))-11) (therefore the results for the CS family are not displayed here). In particular, the SSB bifurcation for the two-layer CS states is present in the interval of values of the inter-layer coupling  $0 < \kappa < \kappa_{\text{max}}^{(\text{CS})} \approx 0.27$ , cf. Figs. 3(c) and 9(c), and Eqs. (23) and (25), for the SV and MM families, respectively.

#### D. Moving solitons

Following Ref. [29], localized states which move steadily at velocity  $\mathbf{v} = (v_x, v_y)$  can be looked for in the form of  $\phi_{\pm} = \phi_{\pm}(x - v_x t, y - v_y t, t)$  and  $\psi_{\pm} = \psi_{\pm}(x - v_x t, y - v_y t, t)$ . The substitution of this in Eq. (1) leads to the equations written in the moving reference frame,

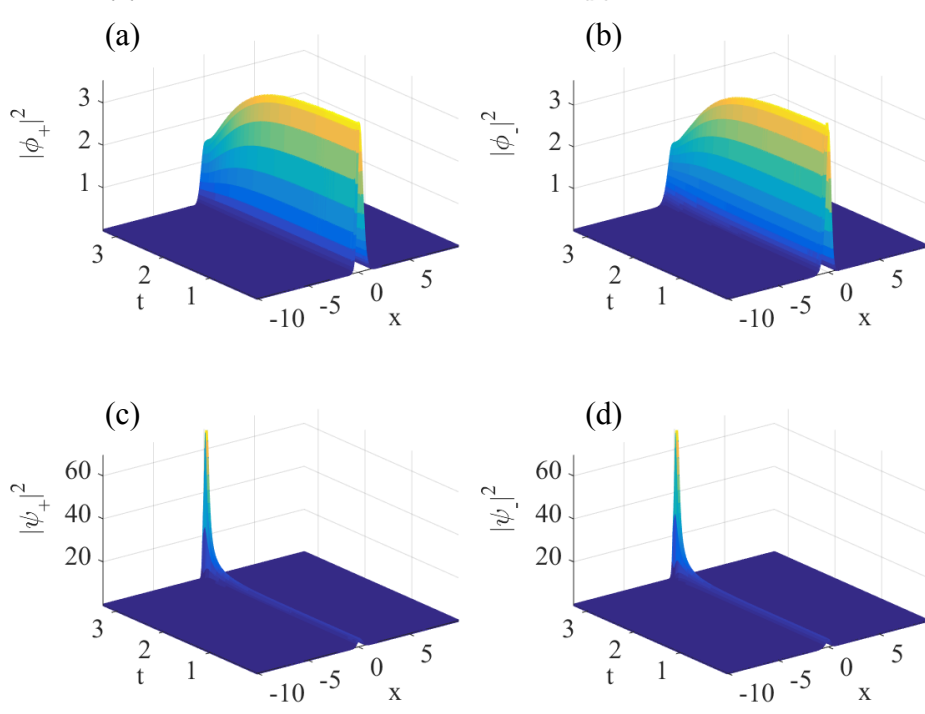


FIG. 11: (Color online) The evolution of an unstable symmetric MM (shown by its density cross-section along  $y = 0$ ) with  $\gamma = 2$ ,  $\kappa = 0.1$ , and  $N = 7.6$ , which belongs to interval (28). In this case, the onset of the SSB quickly leads to the collapse in one layer.

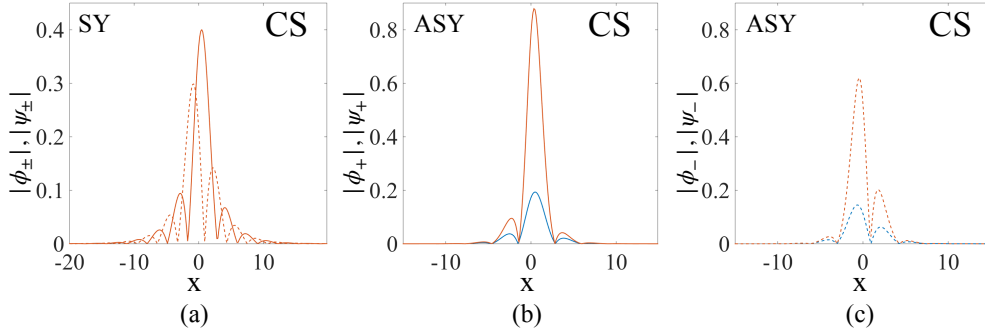


FIG. 12: (Color online) (a) Cross-section profiles (along axis  $y = 0$ ) of a stable symmetric CS (composite soliton) with  $\gamma = 1$  in Eqs. (1),  $N = 3.6$  and  $\kappa = 0.1$ . Values of the angular momentum per particle [defined as per Eq. (29)] for the components are  $(L_{\phi_+}, L_{\phi_-}) = (-0.23, 0.75)$ . The solid and dashed lines designate, respectively,  $|\phi_+| = |\psi_+|$  and  $|\phi_-| = |\psi_-|$ . (b,c) The same profiles for a stable asymmetric CS with  $\gamma = 1$ ,  $N = 4$ , and  $\kappa = 0.1$  (solid and dashed for  $\phi_+$ ,  $\psi_+$  and  $\phi_-$ ,  $\psi_-$ , respectively). In this case, orange and blue curves represent the  $\phi_{\pm}$  and  $\psi_{\pm}$  components, respectively. Angular momenta per particle for the four components are  $(L_{\phi_+}, L_{\phi_-}, L_{\psi_+}, L_{\psi_-}) = (-0.26, 0.72, -0.22, 0.67)$ .

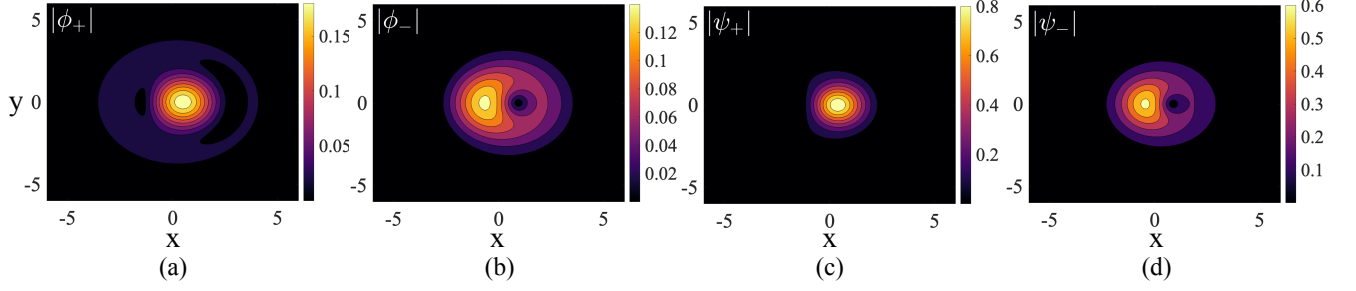


FIG. 13: (Color online) (a) Top-view profiles of components of the asymmetric CS which is presented by its cross-section profiles in Figs. 12(b,c), cf. Fig. 8 for the asymmetric MM.

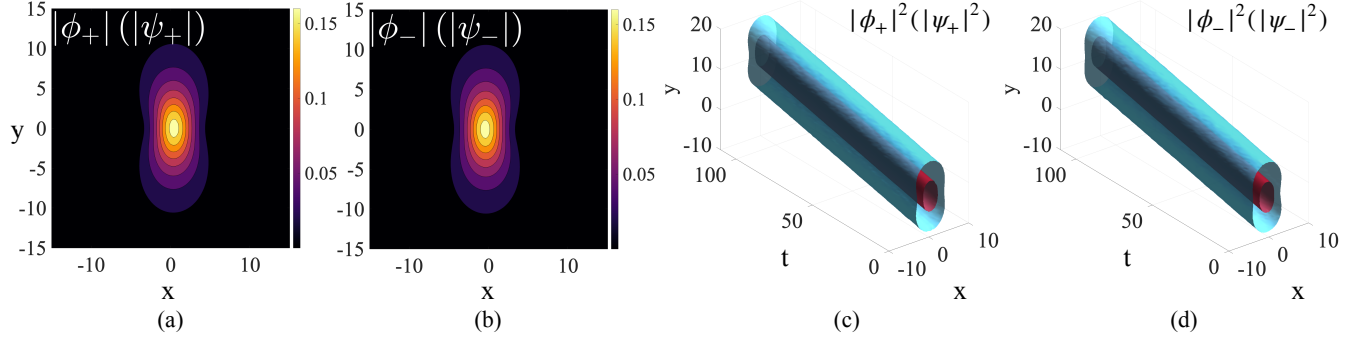


FIG. 14: (Color online) Contour plots of  $|\phi_+(x, y)| = |\psi_+(x, y)|$  (a) and  $|\phi_-(x, y)| = |\psi_-(x, y)|$  (b) of a stable symmetric MM soliton, with  $N = 3$ , and parameters  $\gamma = 2$ ,  $\kappa = 0.1$ , moving at velocity  $(v_y = 0.1, v_x = 0)$ . (c,d) The evolution of the same soliton, simulated in the framework of Eqs. (1) (written in the quiescent coordinates, rather than moving ones), corroborates its stability.

$$\begin{aligned}
 i \frac{\partial \phi_+}{\partial t} - i(\mathbf{v} \cdot \nabla) \phi_+ &= -\frac{1}{2} \nabla^2 \phi_+ - (|\phi_+|^2 + \gamma |\phi_-|^2) \phi_+ + \lambda \left( \frac{\partial \phi_-}{\partial x} - i \frac{\partial \phi_-}{\partial y} \right) - \kappa \psi_+, \\
 i \frac{\partial \phi_-}{\partial t} - i(\mathbf{v} \cdot \nabla) \phi_- &= -\frac{1}{2} \nabla^2 \phi_- - (|\phi_-|^2 + \gamma |\phi_+|^2) \phi_- - \lambda \left( \frac{\partial \phi_+}{\partial x} + i \frac{\partial \phi_+}{\partial y} \right) - \kappa \psi_-,
 \end{aligned} \tag{30}$$

$$\begin{aligned}
 i \frac{\partial \psi_+}{\partial t} - i(\mathbf{v} \cdot \nabla) \psi_+ &= -\frac{1}{2} \nabla^2 \psi_+ - (|\psi_+|^2 + \gamma |\psi_-|^2) \psi_+ + \lambda \left( \frac{\partial \psi_-}{\partial x} - i \frac{\partial \psi_-}{\partial y} \right) - \kappa \phi_+, \\
 i \frac{\partial \psi_-}{\partial t} - i(\mathbf{v} \cdot \nabla) \psi_- &= -\frac{1}{2} \nabla^2 \psi_- - (|\psi_-|^2 + \gamma |\psi_+|^2) \psi_- - \lambda \left( \frac{\partial \psi_+}{\partial x} + i \frac{\partial \psi_+}{\partial y} \right) - \kappa \phi_-,
 \end{aligned}$$

where  $x$  and  $y$  actually stand for  $x - v_x t$  and  $y - v_y t$ . Stationary solutions to these equations have been obtained by means of the same AITEM technique which was also used, as mentioned above, for producing quiescent solitons. As well as in Ref. [29], moving MMs are robust states, surviving up to relatively high speeds, before they undergo delocalization at a critical value of the speed. In particular, setting, as above,  $\gamma = 2$  in Eqs. (30), a typical example of a stable moving symmetric MM soliton is displayed in Fig. 14, for

$$(N, \kappa) = (3, 0.1) \tag{31}$$

and  $(v_x, v_y) = (0, 0.1)$ . Panels (c,d) of the figure corroborate the stability of the moving soliton, whose stationary shape is displayed in panels (a,b).

Note that the quiescent MM soliton with the same values of the parameters as given by Eq. (31), is unstable against the SSB, as seen in Fig. 10, unlike the stable moving soliton in Fig. 14. This means that motion helps to stabilize the symmetric MMs against the symmetry breaking. Effects of the motion are summarized in Fig. 15(a), which shows

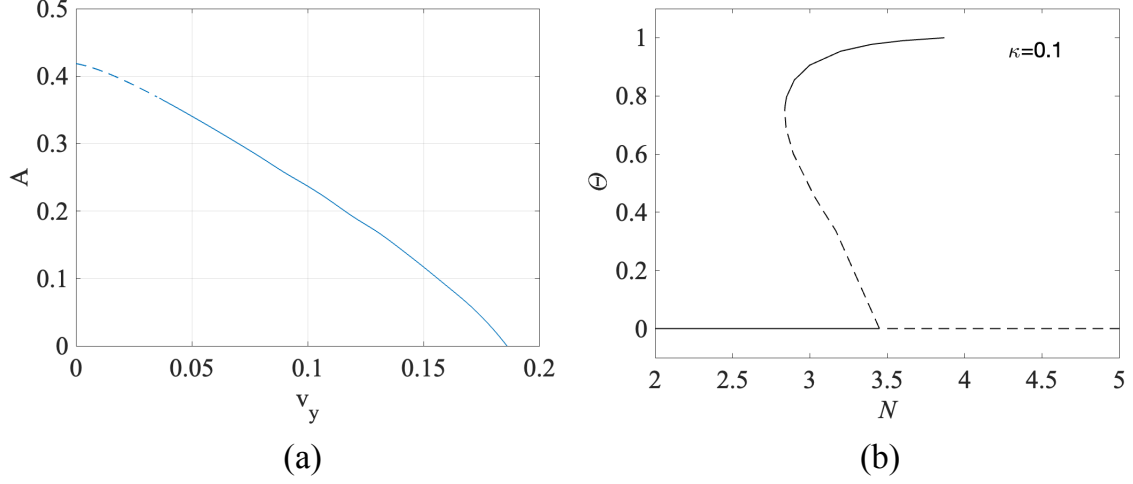


FIG. 15: (Color online) (a) The amplitude of the moving symmetric MM soliton as a function of its velocity,  $v_y$ , for the fixed total norm and inter-layer coupling constant,  $N = 3$  and  $\kappa = 0.1$ . (b) The symmetry-breaking bifurcation of the moving 2D two-layer MMs, for the same  $\kappa = 0.1$  and fixed velocity  $v_y = 0.1$ . In both panels (a) and (b), solid and dashed curves designate stable and unstable solutions, respectively. These plots are produced for  $\gamma = 2$  in Eqs. (30).

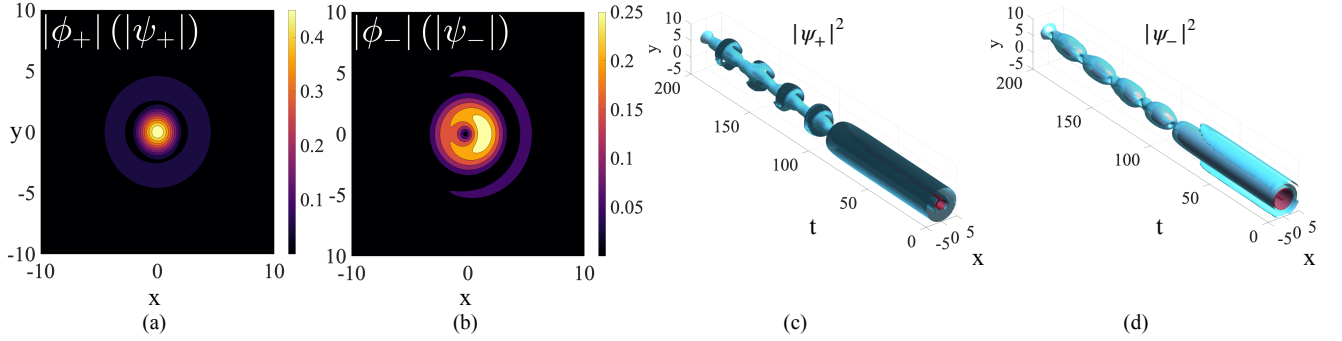


FIG. 16: (Color online) Contour plots of  $|\psi_+(x, y)|$  (or  $|\phi_+(x, y)|$ ) (a) and  $|\psi_-(x, y)|$  (or  $|\phi_-(x, y)|$ ) (b) of a stable symmetric SV soliton with  $N = 5$  and  $\kappa = 0.1$ , moving at velocity  $v_y = 0.005$  (while  $v_x = 0$ ). (c,d) The evolution of an unstable symmetric SV soliton with  $(N, \kappa, v_y) = (5.6, 0.1, 0.005)$ , produced by simulations of Eq. (1). It shows the onset of the spontaneous symmetry breaking with concomitant oscillations. The unstable soliton keeps traveling in the  $y$  direction at the initial velocity,  $v_y = 0.005$ .

the amplitude of the moving symmetric MM, defined as

$$A = \sqrt{|\phi_+(0, 0)|^2 + |\phi_-(0, 0)|^2} \equiv \sqrt{|\psi_+(0, 0)|^2 + |\psi_-(0, 0)|^2} \quad (32)$$

(in the moving coordinates), vs.  $v_y$ . First, we note that, as said above, the symmetric MM soliton is unstable at  $v_y = 0$ , and the increase of the velocity leads to the stabilization at  $v_y \approx 0.03$ . Further, amplitude (32) *monotonically decreases* with the growth of the velocity, and the soliton vanishes, through delocalization, at a critical speed,

$$(v_y)_{\max}^{(\text{MM})} \approx 0.18. \quad (33)$$

The conclusion concerning the robustness of the moving MM solitons is in qualitative agreement with the finding displayed above in Fig. 10, which demonstrates that the SSB transforms unstable MMs into stably drifting breathers.

The SSB of the moving MM solitons, with fixed velocity  $v_y = 0.1$ , is summarized in Fig. 15(b) by means of the respective symmetry-breaking diagram, which shows asymmetry parameter (13) vs. the total norm,  $N$ , defined as above [according to Eq. (12)]. In this case, the SSB point is  $N_{\text{cr}} \approx 3.5$ , which is essentially larger than its counterpart,  $N_{\text{cr}} \approx 2.8$ , found above for the quiescent MM solitons, cf. Fig. 9(b). This finding corroborates the above conclusion,

that the motion helps to stabilize the MM solitons against the SSB. It is worthy to note that the SSB bifurcation for the moving solitons always remains subcritical.

Although Eqs. (30) seem anisotropic in the  $(x, y)$  plane, the numerical analysis of the MM solitons moving in the  $x$  direction produces the same results, as concerns the dependences between the amplitude and velocity, and the SSB diagram, as shown in Fig. 15 for the solitons moving along the  $y$  axis. Thus, the system is actually isotropic for moving solitons (this point was not considered in Ref. [29]).

Unlike the MMs, moving SV solitons are fragile, suffering delocalization at small values of the velocity (for the single-layer system, this conclusion was made in Ref. [29]). For example, at parameters  $\gamma = 0$  and  $\kappa = 0.1$ , the moving SVs with norms  $N = 5$  and  $7.4$  exist up to the critical speeds  $(v_y)_{\max}^{(SV)}(N = 5) \approx 0.01$  and  $(v_y)_{\max}^{(SV)}(N = 7.4) \approx 0.03$ , respectively, cf. the much larger critical speed (33) for the moving MMs. At  $|v_y| > (v_y)_{\max}^{(SV)}$ , numerical solution to Eqs. (30), produced by AITEM, does not demonstrate delocalization. Instead, the moving SVs convert into MM states, instead of SVs. This conclusion also agrees with the findings for the single-layer system, reported in Ref. [29].

A typical example of a stably moving symmetric SV is presented in Figs. 16(a,b) for  $(N, \kappa, \gamma) = (5, 0.1, 0)$  and  $v_y = 0.005$ . Panels (c) and (d) of the figure display the evolution of an initially symmetric SV with  $(N, \kappa, \gamma) = (5.6, 0.1, 0)$  and the same speed,  $v_y = 0.005$ , which is unstable against SSB, due to the slightly larger value of the total norm. It is seen that the dynamical symmetry breaking sets in along with concomitant oscillations. Generally, this is similar to the SSB-induced instability in the quiescent SVs, cf. Fig. 4.

It is relevant to note that the shape of the SV soliton moving along the  $y$  axis, which is displayed in Fig. 16, keeps spatial symmetry with respect to the  $x$  axis, and features conspicuous asymmetry with respect to  $y$  (the same asymmetry, but in a weaker form, is observed for moving SV solitons in Fig. 16, as well as in Ref. [29]). The distortion of the axial symmetry of the quiescent SV solitons (see Fig. 2) under the action of motion is a manifestation of the Magnus effect for vortex solitons, cf. Rev. [51].

#### IV. CONCLUSION

The objective of this work is to extend the analysis of 2D solitons supported by the interplay of the cubic self- and cross-attraction and linear SOC (spin-orbit coupling) in the model of the binary BEC. A surprising result, first reported in Ref. [29], was that this system gives rise to absolutely stable 2D solitons of the SV (semi-vortex), MM (mixed-mode), and CS (composite-soliton) types, the latter one only existing in the case of the Manakov's nonlinearity. These solitons furnish the system's ground state, which does not exist in the absence of the SOC terms (in that case, the collapsing regime formally plays the role of the ground state). In the present work, we aimed to consider the double-layer setting, in which two identical nonlinear systems stabilized by SOC are linearly coupled by tunneling of atoms. Stationary solutions of the two-layer model were produced by means of AITEM (accelerated imaginary-time evolution method), and their stability was tested by means of direct real-time simulations.

It has been concluded that the 2D solitons of the SV, MM, and CS types, which are initially symmetric with respect to the tunnel-coupled layers, are subject to the SSB (spontaneous-symmetry-breaking) bifurcation, which is always of the subcritical type. Branches of stable asymmetric 2D solitons, produced by the SSB bifurcation, exist up to the value of the total norm equal to that of the TSs (Townes solitons), as the collapse takes place at norms exceeding the TS value. This picture is valid up to a certain largest value of the inter-layer coupling constant; above that value, the bifurcation does not take place, because the collapse commences prior to it. The evolution of initially symmetric 2D solitons of the SV and MM types, which are destabilized by the SSB, features dynamical symmetry breaking, along with the establishment of intrinsic oscillations of the soliton, or quick development of the collapse, if the total norm is large enough to drive the collapse. In the case of MMs, the breather produced by the symmetry-breaking instability features spontaneous drift, in addition to the intrinsic oscillations.

Moving 2D solitons were investigated in the traveling reference frame. This is a relevant problem because the SOC breaks the system's Galilean invariance. It has been found that moving MMs are robust 2D solitons, which exist up to the critical value of the velocity, above which they suffer delocalization. Traveling SVs are fragile states, for which the critical speed is very small. Above it, the solitons do not decay, but spontaneously rearrange themselves into moving MM state. This phenomenon was also observed in a single-layer model in Ref. [29].

To extend the present work, it may be relevant to study interactions between the stable 2D solitons. This problem should be especially interesting for interactions between stable asymmetric solitons. Additionally, it is also interesting to consider initially asymmetric pair of layers with unequal SOC strengths  $\lambda$  in them. Consideration of the nonlinear interaction between the layers, in addition to the linear coupling, may be relevant too.

## Acknowledgments

We appreciate valuable discussions with H. Sakaguchi. This work was supported, in part, by the Israel Science Foundation through grant No. 1695/22, and in part, by Key Research Projects of General Colleges in Guangdong Province through grant No. 2019KZDXM001. Z.C. acknowledges a fellowship provided by the Helen Diller quantum center at the Technion (Haifa, Israel).

- 
- [1] Hauk P, Cucchiatti FM, Tagliacozzo L, Deutsch I, Lewenstein M. Can one trust quantum simulators?. *Rep. Prog. Phys.* 2012; 75:082401.
  - [2] Dresselhaus G. Spin-orbit coupling effects in zinc blende structures. *Phys. Rev.* 1955;100:580-586.
  - [3] Bychkov YA, Rashba EI. Oscillatory effects and the magnetic susceptibility of carriers in inversion layers. *J. Phys. C: Solid State Phys.* 1984;17:6039-6045.
  - [4] Lin YJ, Jiménez-García K, Spielman IB. Spin-orbit-coupled Bose-Einstein condensates. *Nature* 2011;471:83-86.
  - [5] Campbell DL, Juzeliūnas G, Spielman IB. Realistic Rashba and Dresselhaus spin-orbit coupling for neutral atoms. *Phys. Rev. A* 2011;84:025602.
  - [6] Galitski V, Spielman IB. Spin-orbit coupling in quantum gases. *Nature* 2013;494:49-54.
  - [7] Lan ZH, Öhberg P. Raman-dressed spin-1 spin-orbit-coupled quantum gas. *Phys. Rev. A* 2014;89:023630.
  - [8] Zhai H. Degenerate quantum gases with spin-orbit coupling: a review. *Rep. Prog. Phys.* 2015;78:026001.
  - [9] Wu Z, Zhang L, Sun W, Xu XT, Wang BZ, Ji SC, Deng Y, Chen S, Liu XJ, Pan JW. Realization of two-dimensional spin-orbit coupling for Bose-Einstein condensates. *Science* 2016;354:83-86.
  - [10] Kawakami T, Mizushima T, Machida K. Textures of  $F = 2$  spinor Bose-Einstein condensates with spin-orbit coupling. *Phys. Rev. A* 2011;84:011607(R).
  - [11] Ramachandran B, Opanchuk B, Liu XJ, Pu H, Drummond PD, Hu H. Half-quantum vortex state in a spin-orbit-coupled Bose-Einstein condensate. *Phys. Rev. A* 2012;85:023606.
  - [12] Sakaguchi H, Li B. Vortex lattice solutions to the Gross-Pitaevskii equation with spin-orbit coupling in optical lattices. *Phys. Rev. A* 2013;87:015602.
  - [13] Conduit GJ. Line of Dirac monopoles embedded in a Bose-Einstein condensate. *Phys. Rev. A* 2012;86:021605(R) .
  - [14] Wu CJ, Mondragon-Shem I, Zhou XF. Unconventional Bose-Einstein condensations from spin-orbit coupling. *Chin. Phys. Lett.* 2011;28:097102.
  - [15] Kawakami T, Mizushima T, Nitta M, Machida K. Stable Skyrmions in  $SU(2)$  gauged Bose-Einstein condensates. *Phys. Rev. Lett.* 2012;109:015301.
  - [16] Achilleos V, Frantzeskakis DJ, Kevrekidis PG, Pelinovsky DE. Matter-wave bright solitons in spin-orbit coupled Bose-Einstein condensates. *Phys. Rev. Lett.* 2013;110:264101.
  - [17] Malomed BA. Polarization dynamics and interactions of solitons in a birefringent optical fiber. *Phys. Rev. A* 1991;43:410-423.
  - [18] Rechtsman MC, Zeuner JM, Plotnik Y, Lumer Y, Podolsky D, Dreisow F, Nolte S, Segev M, Szameit A. Photonic Floquet topological insulators. *Nature* 2013;496:196-200.
  - [19] Bergé L. Wave collapse in physics: principles and applications to light and plasma waves. *Phys. Rep.* 1998;303:259-372.
  - [20] Sulem C, Sulem PL. *The Nonlinear Schrödinger Equation: Self-Focusing and Wave Collapse.* New York: Springer; 2007.
  - [21] Zakharov VE, Kuznetsov EA. Solitons and collapses: two evolution scenarios of nonlinear wave systems. *Physics - Uspekhi* 2012;55:535-556.
  - [22] Fibich G. *The nonlinear Schrödinger equation: singular solutions and optical collapse.* Heidelberg: Springer; 2015.
  - [23] Malomed BA. (INVITED) Vortex solitons: Old results and new perspectives. *Physica D* 2019;399:108-137.
  - [24] Chiao RY, Garmire E, Townes CH. Self-trapping of optical beams. *Phys. Rev. Lett.* 1964;13:479-82.
  - [25] Kruglov VI, Logvin YA, Volkov VM. The theory of spiral laser beams in nonlinear media. *J. Mod. Phys.* 1992; 39: 2277-2291.
  - [26] Kruglov VI, Vlasov RA. Spiral self-trapping propagation of optical beams. *Phys. Lett. A* 1985;111:401-404.
  - [27] Kruglov VI, Volkov VM, Vlasov RA, Drits VV. Auto-waveguide propagation and the collapse of spiral light beams in non-linear media. *J. Phys. A: Math. Gen.* 1988;21:4381-4395.
  - [28] Mardonov S, Sherman EY, Muga JG, Wang HW, Ban Y, Chen, X. Collapse of spin-orbit-coupled Bose-Einstein condensates. *Phys. Rev. A.* 2015;91:043604.
  - [29] Sakaguchi H, Li B, Malomed BA. Creation of two-dimensional composite solitons in spin-orbit-coupled self-attractive Bose-Einstein condensates in free space. *Phys. Rev. E* 2014;89:032920.
  - [30] Sakaguchi H, Malomed BA. Discrete and continuum composite solitons in Bose-Einstein condensates with the Rashba spin-orbit coupling in one and two dimensions. *Phys. Rev. E* 2014;90:062922.
  - [31] Salasnich L, Cardoso WB, Malomed BA. Localized modes in quasi-two-dimensional Bose-Einstein condensates with spin-orbit and Rabi couplings. *Phys. Rev. A* 2014;90:033629.
  - [32] Sakaguchi H, Sherman EYa, Malomed BA. Vortex solitons in two-dimensional spin-orbit coupled Bose-Einstein condensates: Effects of the Rashba-Dresselhaus coupling and the Zeeman splitting. *Phys. Rev. E* 2016;94:032202.
  - [33] Sherman EYa. Random spin-orbit coupling and spin relaxation in symmetric quantum wells. *Appl. Phys. Lett.* 2003;82:209-



211.

- [34] Manakov SV. On the theory of two-dimensional stationary self-focusing of electromagnetic waves. *Zh. Eksp. Teor. Fiz.* 1973;65: 505-516 [Sov. Phys. JETP 1974;38:248-253].
- [35] Chen Z, Li Y, Malomed BA. Josephson oscillations of chirality and identity in two-dimensional solitons in spin-orbit-coupled condensates. *Phys. Rev. Research* 2020;2:033214.
- [36] Wright EM, Stegeman GI, Wabnitz S. Solitary-wave decay and symmetry-breaking instabilities in two-mode fibers. *Phys. Rev. A* 1989;40:4455.
- [37] Iooss G, Joseph DD. *Elementary Stability Bifurcation Theory*. New York: Springer; 1980.
- [38] Paré C, Florjańczyk M. Approximate model of soliton dynamics in all-optical fibers. *Phys. Rev. A* 1990;41:6287-6295.
- [39] Maimistov AI. Propagation of a light pulse in nonlinear tunnel-coupled optical waveguides. *Sov. J Quantum Electron* 1991;21:687-690.
- [40] Akhmediev N, Ankiewicz A. Novel soliton states and bifurcation phenomena in nonlinear fiber couplers. *Phys. Rev. Lett.* 1993;70:2395-2398.
- [41] Malomed BA, Skinner I, Chu PL, Peng GD. Symmetric and asymmetric solitons in twin-core nonlinear optical fibers. *Phys. Rev. E* 1996;53:4084.
- [42] Nguyen VH, Tai LXT, Bugar I, Longobucco M, Buzcynski R, Malomed BA, Trippenbach M. Reversible ultrafast soliton switching in dual-core highly nonlinear optical fibers. *Opt. Lett.* 2020;45:5221-5224.
- [43] Gubeskys A, Malomed BA. Symmetric and asymmetric solitons in linearly coupled Bose-Einstein condensates trapped in optical lattices. *Phys. Rev. A* 2007;75:063602.
- [44] Matuszewski M, Malomed BA, Trippenbach M. Spontaneous symmetry breaking of solitons trapped in a double-channel potential. *Phys. Rev. A* 2007;75:063621.
- [45] Milburn GJ, Corney J, Wright EM, Walls DF. Quantum dynamics of an atomic Bose-Einstein condensate in a double-well potential. *Phys. Rev. A* 1997;55:4318-4324.
- [46] Smerzi A, Fantoni S, Giovanazzi S, Shenoy SR. Quantum coherent atomic tunneling between two trapped Bose-Einstein condensates. *Phys. Rev. Lett.* 1997;79:4950-4953.
- [47] Albiez M, Gati R, Fölling J, Hunsmann S, Cristiani M, Oberthaler MK. Direct observation of tunneling and nonlinear self-trapping in a single bosonic Josephson junction. *Phys. Rev. Lett.* 2005;95:010402.
- [48] Chen Z, Li Y, Malomed BA, Salasnich L. Spontaneous symmetry breaking of fundamental states, vortices, and dipoles in two and one-dimensional linearly coupled traps with cubic self-attraction. *Phys. Rev. A* 2017;96:033621.
- [49] Yang J, Lakoba TI. Accelerated imaginary-time evolution methods for the computation of solitary waves. *Stud. Appl. Math.* 2008;120:265292.
- [50] Vakhitov NG, Kolokolov AA. Stationary solutions of the wave equation in a medium with nonlinearity saturation. *Radio-phys. Quantum Electron.* 1973;16:783-789.
- [51] Metlitski MA, Zhitnitsky, AR. Vortons in two component Bose-Einstein condensates. *J. High Energy Phys.* 2004;6:017.